A Template-Assembled Synthetic Protein Surface Mimetic of the von Willebrand Factor A1 domain Inhibits Botrocetin-Induced Platelet Aggregation

Jacques Hauert,[a] Jimena Fernandez-Carneado,[c] Olivier Michielin,[d] Stéphane Mathieu,[a] Daniel Grell,[c] Marc Schapira,[a] Olivier Spertini,[a] Manfred Mutter,[c] Gabriele Tuchscherer,[c] and Tibor Kovacsovics*[a, b]

Platelet adhesion, the initial step of platelet activation, is mediated by the interaction of von Willebrand factor (VWF) with its platelet receptor, the GPIb–IX complex. The binding of VWF to GPIb–IX is induced either by increased shear stress or by exogenous modulators, such as botrocetin. At a molecular level, this interaction takes place between the A1 domain of VWF and the GPIbα chain of the GPIb–IX complex. We report here the design and functional characteristics of a VWF template-assembled synthetic protein (TASP), a chimeric four-helix-bundle TASP scaffold mimicking the surface of the A1 domain. Twelve residues located on helices α3 and α4 in the native A1 domain were grafted onto a surface formed by two neighboring helices of the TASP. VWF TASP was found to inhibit specifically botrocetin-induced platelet aggregation and to bind both botrocetin and GPIbα. However, in contrast to the native A1 domain, VWF TASP did not bind simultaneously to both ligands. Modeling studies revealed that the relative orientation of the α helices in VWF TASP led to a clash of bound botrocetin and GPIbα. These results demonstrate that a chimeric four-helix-bundle TASP as a scaffold offers a suitable surface for presenting crucial residues of the VWF A1 domain; the potential of the TASP approach for de novo protein design and mimicry is thereby illustrated.

Introduction

Von Willebrand factor (VWF) is a multimeric adhesive glycoprotein that plays a central role in hemostasis and thrombosis by initiating platelet adhesion to injured subendothelium and recruiting additional platelets to the growing thrombus.[1,2] In vivo, platelet adhesion is mediated by the interaction between surface-bound VWF and the GPIbα chain of the GPIb–IX complex. This interaction does not occur in the circulation and is thought to require a conformational change in VWF, which can be induced by increased shear stress conditions.[3] A high-affinity binding site on VWF for GPIbα can also be induced by exogenous modulators, such as ristocetin or botrocetin.[4,5] However, shear stress, ristocetin, and botrocetin may induce distinct binding sites on VWF for GPIbα. Indeed, recent evidence suggests that the binding site mediated by ristocetin is more closely related to that induced by shear stress than to the botrocetin-mediated binding site.[6–8]

The functional domain organization of VWF is well-characterized.[9] The binding site for GPIbα is mapped to the A1 domain of VWF, which extends between residues 497 and 716 of the mature VWF subunit and is also involved in interactions of VWF with botrocetin, heparin, and sulfatides. The three-dimensional structure of the VWF A1 domain has been determined by X-ray crystallography.[10,11] The A1 domain is composed of a central β sheet formed by six β strands that is surrounded by six α helices. The putative GPIbα interaction site was initially thought to span a surface formed by the parallel helices α3 and α4, as well as a groove with the neighboring strand β3.[7,12–14] The crystal structures of the GPIbα–A1 complex[15] and of the botrocetin–A1 complex[16] have been described recently. The interaction between GPIbα and the A1 domain involves, in fact, two binding sites: a large site formed by helix α3, loop α3–β4, and strand β3 and a smaller site formed by loops α1–β3, β3–α2 and α3–β4.[15] The binding site for botrocetin spans helices α4 and α5.[7,16,17]

An important development in de novo protein design is based on the use of protein or peptide scaffolds for the intro-

[a] *Dr. J. Hauert,[#] S. Mathieu, Prof. Dr. M. Schapira, Prof. Dr. O. Spertini, Dr. T. Kovacsovics*
Hematology Service, Centre Hospitalier Universitaire Vaudois
1011 Lausanne (Switzerland)
Fax: (+41) 21-314-0791

[b] *Dr. T. Kovacsovics*
Current address:
Center for Hematological Malignancies, OHSU
3181 SW Sam Jackson Park Road
Mail code UHN73C, Portland, OR 97239 (USA)
Fax: (+1) 503-494-1552
E-mail: kovacsov@ohsu.edu

[c] *Dr. J. Fernandez-Carneado,[#] Dr. D. Grell, Prof. Dr. M. Mutter, Priv.-Doz. Dr. G. Tuchscherer*
Institute of Organic Chemistry, EPFL
1015 Lausanne (Switzerland)

[d] *Dr. O. Michielin*
Ludwig Institute and Swiss Institute of Bioinformatics
1066 Epalinges (Switzerland)

[#] *These authors contributed equally to this manuscript.*

  DOI: 10.1002/cbic.200300826

duction and stabilization of protein functional domains.[18,19] The key feature of the concept of template-assembled synthetic proteins (TASPs) is that it allows for template-directed self-assembly of α-helical and/or β-sheet peptide blocks into stable protein-like folding units.[20–22] The resulting constructs offer a suitable area for the spatial arrangement of discontinuous binding residues that are in close proximity upon folding in the native protein.

We report here the design and functional characteristics of a TASP mimicking the three-dimensional structure of the VWF A1 domain. Our goal was to produce a TASP exhibiting at its surface, in an adequate orientation, twelve selected residues from helices α3 and α4 of the A1 domain. This task was achieved by incorporating these residues at specific locations of a template-anchored homodimeric four-helix bundle, based on the structure of ROP (repressor of primer), a homodimeric protein of relatively high stability and resistance to mutations.[23] The TASP obtained by this approach, the VWF TASP, was found to inhibit specifically botrocetin-induced platelet aggregation and to bind both GPIbα and botrocetin. However, in contrast to the native A1 domain, VWF TASP could not bind these inducers simultaneously. Modeling studies, based on the recently described crystal structures of the GPIbα–A1 and botrocetin–A1 complexes, have explained the structural basis of these results.

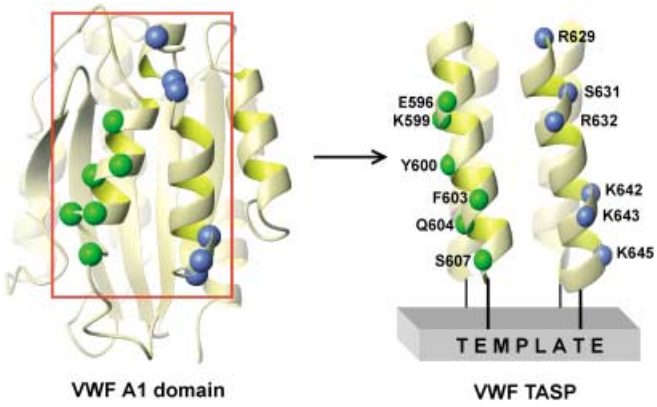

Figure 1. *Grafting of a molecular surface of the A1 domain of VWF onto a four-helix-bundle TASP scaffold. Left: Ribbon representation of the A1 domain of VWF with selected residues of helix αI depicted in blue and of helix αII depicted in green. Right: Two neighboring helices in the TASP molecule provide an adequate scaffold to accommodate the same residues in the appropriate geometry.*

Results

Design and synthesis of VWF TASP

Earlier studies with X-ray crystallography and alanine scans have identified a series of amino acid residues, located on the parallel helices α3 and α4 of the VWF A1 domain, that appear to be involved in direct contacts with GPIbα.[10,11,24,25] In this study, we have designed, using the TASP concept, a chimeric protein that mimics the surface defined by these residues. To do this, we chose as the scaffold a symmetrical tetramer called symROP A_4L_4, developed in Mutter's laboratory,[26] which has been derived from the core structure of ROP, a homodimeric protein of relatively high stability and tolerance to mutations that is composed of two helical hairpin units.[23] In this construct, the α helices are arranged in an antiparallel fashion and the core residues of ROP (Leu, Ala) ensure favorable hydrophobic interactions in the interior of the four-helix-bundle TASP. Residues that are nonessential for bundle stabilization, pointing to the external surface, can be substituted by residues forming the surface that is being mimicked. In this study, six residues of VWF helix α4 (Arg629, Ser631, Arg632, Lys642, Lys643, and Lys645) were incorporated into the helix sequence αI of symROP A_4L_4 and six residues of helix α3 (Glu596, Lys599, Tyr600, Phe603, Gln604, and Ser607) were incorporated into helix αII (Figure 1). To stabilize the formation of the four-helix-bundle structure, the four helices were sequentially attached to a cyclic decapeptide template by chemoselective ligation. To further increase the stability of this structure in a locked-in conformation,[27] a disulfide bond was formed between the two αI helices at the site opposite to the template (Figure 2). CD spectroscopic investigation in aqueous phosphate buffer revealed a high helical content and a significant increase in secondary-structure formation, due to the template-inducing long-range interactions of the attached helices, that is indicative of the proposed helix-bundle structure (Figure 3). The CD spectrum of this TASP shows the characteristic bands of a helix conformation, that is, two negative Cotton

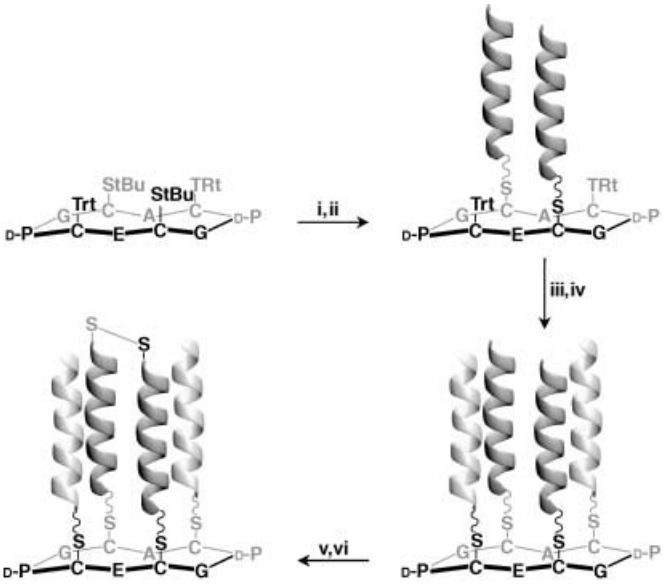

Figure 2. *Synthesis of VWF-TASP. The antiparallel attachment of the four helices was achieved by selective thioether formation. Orthogonal protecting groups of the four Cys residues (StBu or Trt) in the cyclic peptide template were removed selectively and the helices were ligated sequentially in aqueous phosphate buffer by using completely unprotected peptide fragments functionalized either at the N or C terminus with a bromoacetic acid moiety; i) removal of StBu; ii) attachment of helix αI through the N terminus; iii) removal of Trt; iv) ligation of helix αII through the C terminus; v) removal of Acm from the N-terminal Cys residue of helix αI; vi) disulfide bond formation. StBu = tert-butylthio, Trt = trityl = triphenylmethyl, Acm = acetamidomethyl.*

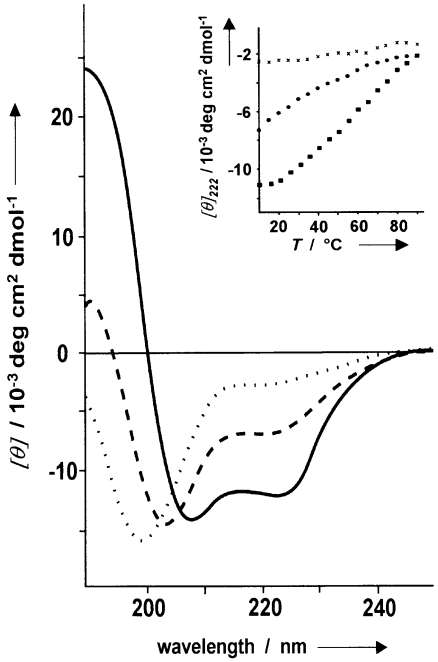

Figure 3. Comparison of the CD spectra (c = 10^{-5} M in phosphate buffer, pH 7) of the individual α helices (dashed lines) and the final disulfide-bridged TASP molecule (solid line) demonstrates the helix-inducing effect of the template as a prerequisite for stable four-helix-bundle formation. Inset: thermal denaturation studies reveal a sigmoidal profile for the TASP molecule (■) indicative of a cooperative unfolding process, in contrast to individual helices (● and ×).

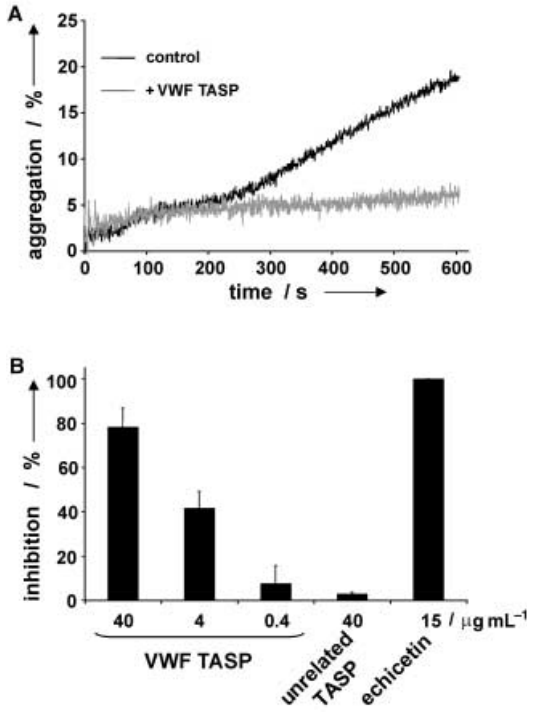

Figure 4. The effect of VWF TASP on botrocetin-induced platelet aggregation. A) Platelet activation by botrocetin. Washed platelets were aggregated in the presence of VWF (10 μg mL^{-1}) and botrocetin (6 μg mL^{-1}), in the presence or absence of VWF TASP (40 μg mL^{-1}). Results are representative of 4–6 experiments. B) Dose-response and specificity of VWF TASP inhibition on botrocetin-induced platelet aggregation. Washed platelets were aggregated in the presence of VWF (10 μg mL^{-1}) and botrocetin (6 μg mL^{-1}), in the presence of increasing doses of VWF TASP, of an unrelated TASP (40 μg mL^{-1}), or of echicetin (15 μg mL^{-1}). Results are expressed as percentage inhibition of platelet aggregation and represent the mean ± standard deviation (SD, n = 5).

effects at $\lambda = 208$ and 222 nm, whereas the individual helices adopt primarily a random-coil structure. Thermal denaturation studies show that, with increasing temperature, the relative ellipticities of the TASP at $\lambda = 222$ nm describe a sigmoid curve, a result indicating a cooperative unfolding of the molecule that is characteristic for globular proteins (Figure 3, inset). The final construct, called VWF TASP, thus contains two identical surfaces, each of them mimicking the topography of a partial surface created by helices α3 and α4 in the native VWF A1 domain.

VWF TASP inhibits botrocetin-induced platelet aggregation

Screening experiments evaluating the effect of VWF TASP on VWF-induced platelet activation included measures of aggregation responses to ristocetin and botrocetin, two compounds that bind directly to the A1 domain of VWF and induce the expression of a binding site for GPIbα.[4,5] VWF TASP prevented botrocetin-induced platelet aggregation (Figure 4A) but had no effect on ristocetin-induced aggregation (data not shown). Inhibition of botrocetin-induced platelet aggregation was dependent on the concentration of VWF TASP, with an IC_{50} value of 6.5 μg mL^{-1} (0.67 μM). At a VWF TASP concentration of 40 μg mL^{-1}, the inhibition was 80% of the inhibition seen with echicetin, a snake venom protein that inhibits GPIbα (Figure 4B). The specificity of VWF TASP inhibition of botrocetin-induced platelet aggregation was demonstrated by a lack of inhibition observed with an unrelated TASP, which was based on the structure of the endothelial cell adhesion molecule E-selectin and shared the same scaffold as VWF TASP (Figure 4B). Also, VWF TASP had no inhibitory effect on platelet activation mediated by thrombin-receptor activating peptide (TRAP) or collagen, observations indicating that VWF TASP does not affect platelet reactions mediated by GPIIb–IIIa (data not shown). Additional studies demonstrated that VWF TASP did not prevent platelet adhesion to VWF either under static conditions or at shear-stress levels of 60 dynes cm^{-2} (data not shown). Taken together, these results indicate that VWF TASP functions as a selective inhibitor of botrocetin-mediated platelet activation, but that this effect does not extend to ristocetin-induced platelet aggregation or to platelet adhesion to VWF under static or flow conditions.

VWF TASP inhibits VWF binding to platelets and GPIbα

The issue of whether VWF TASP prevented the interaction of VWF with the GPIb–IX complex on platelets was examined in binding experiments employing ^{125}I-VWF. VWF TASP inhibited in a concentration-dependent fashion the binding of ^{125}I-VWF to washed platelets whereas the unrelated TASP had no effect (Figure 5A). For example, at a concentration of 120 μg mL^{-1},

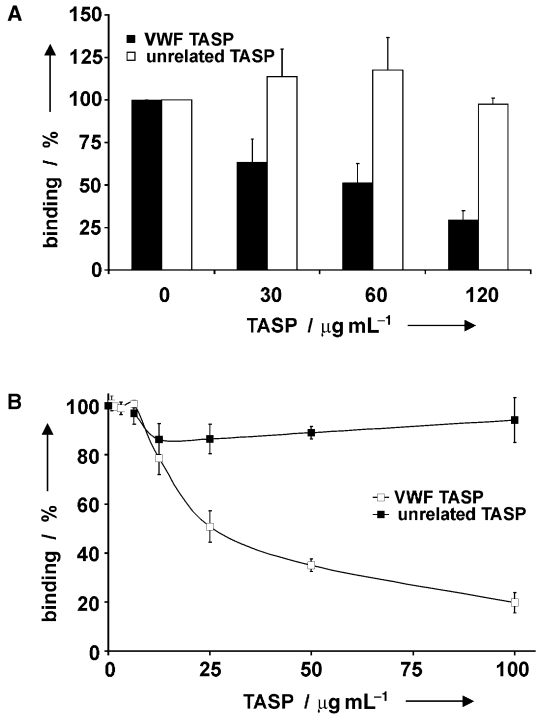

Figure 5. Effect of VWF TASP on VWF binding to platelets and to glycocalicin. A) Washed platelets were incubated with ^{125}I-VWF and botrocetin in the presence of increasing doses of VWF TASP or of an unrelated TASP for 30 minutes. The results are expressed as percentage binding compared to the maximal binding, which was defined as the binding of VWF in the absence of inhibitor, and represent the mean ±SD (n=4). B) ELISA plates coated with glycocalicin were incubated with biotin-labeled VWF (5 μg mL^{-1}) in the presence of botrocetin and increasing doses of VWF TASP or of an unrelated TASP. The reaction was revealed by the addition of steptravidin-bound horse radish peroxidase and o-phenylenediamine. The results are expressed as percentage binding compared to the maximal binding, which was defined as the binding of VWF in the absence of inhibitor, and represent the mean ±SD (n=5).

VWF TASP decreased ^{125}I-VWF binding to platelets to 70% of that seen in the absence of inhibitor. No binding inhibition was detected when using free αI and αII helices (data not shown), a result indicating that the incorporation of the helices in VWF TASP stabilizes the overall structure of the complex. Additional investigations examined the binding of biotinylated VWF to GPIbα by using a solid-phase binding assay employing immobilized glycocalicin, the soluble extracellular domain of GPIbα. VWF TASP inhibited the binding of biotin-labeled VWF to glycocalicin in a concentration-dependent fashion whereas the unrelated TASP had no effect (Figure 5B). These results demonstrate that VWF TASP inhibits VWF-dependent botrocetin-induced platelet responses by interfering with the interaction between VWF and GPIbα.

VWF TASP interacts with VWF binding sites for botrocetin and GPIbα

The interaction between the GPIb–IX complex on platelets and VWF does not take place under static conditions and requires elevated shear stress conditions or the presence of modulators such as botrocetin or ristocetin. Botrocetin is known to interact with VWF and to induce a binding site for GPIbα.[4] Since VWF TASP was found to inhibit the botrocetin-dependent interaction between VWF and GPIbα, we asked whether it did so by preventing the interaction of botrocetin with VWF, of glycocalicin with VWF, or both reactions. These issues were addressed by using a solid-phase binding assay employing immobilized VWF TASP and biotinylated glycocalicin and botrocetin. Interestingly, both botrocetin and glycocalicin were found to bind directly to VWF TASP and showed saturable binding (Figure 6A and B). This interaction was specific for VWF TASP and it it did

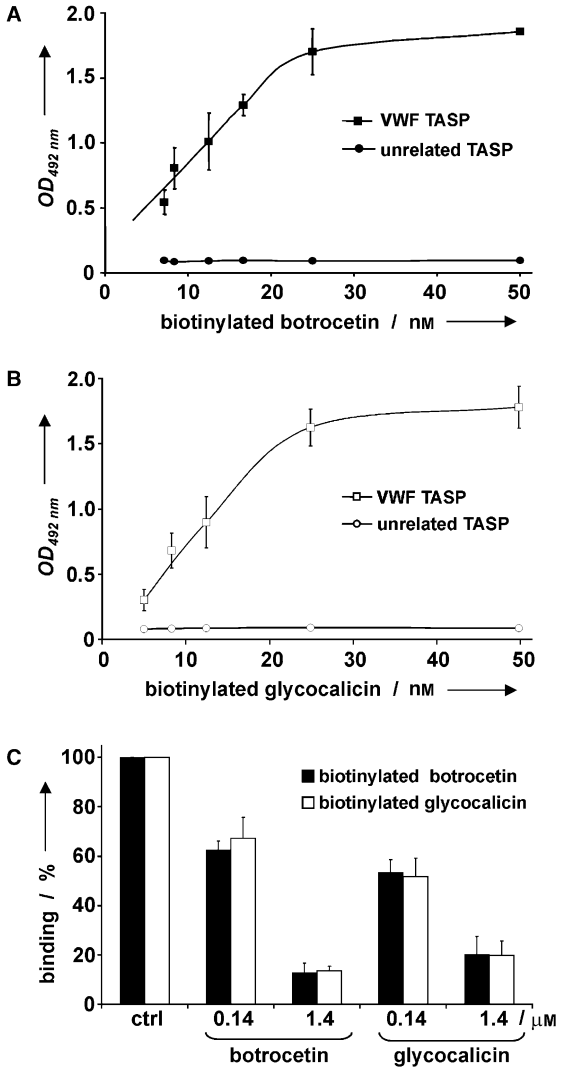

Figure 6. Binding of botrocetin and glycocalicin to VWF TASP. A and B) ELISA plates coated with VWF TASP or with an unrelated TASP were incubated with increasing amounts of biotinylated botrocetin (A) or biotinylated glycocalicin (B). The reaction was revealed by the addition of streptavidin-bound horse radish peroxidase and o-phenylenediamine. The results are expressed as the optical density at 492 nm and represent the mean ±SD (n=4). C) Cross-blocking experiments of the binding of glycocalicin and botrocetin to VWF TASP. ELISA plates coated with VWF TASP were incubated with biotinylated botrocetin (14 nM) or biotinylated glycocalicin (14 nM) in the presence of unlabeled botrocetin (0.14 or 1.4 μM) or unlabeled glycocalicin (0.14 or 1.4 μM). Results are expressed as percentage binding compared to the binding in the absence of inhibitor and represent the mean ±SD (n=4).

not take place with an unrelated TASP. The binding of biotinylated glycocalicin and botrocetin to VWF TASP was inhibited, in a concentration-dependent manner, by unlabeled glycocalicin and botrocetin, respectively, a result indicating that biotinylation of the ligands did not alter their affinity for VWF TASP. Cross-blocking studies showed that the interaction of biotinylated botrocetin or glycocalicin with VWF TASP could be blocked by unlabeled glycocalicin or botrocetin, respectively (Figure 6C). Thus, in contrast to the native A1 domain, which binds glycocalicin and botrocetin at the same time,[4,7] VWF TASP cannot interact simultaneously with both molecules. These results suggest either that the binding sites for botrocetin or glycocalicin on VWF TASP are overlapping or in close proximity in VWF TASP, or that another phenomenon prevents the simultaneous binding of both molecules to VWF TASP.

Structural analysis of VWF TASP interaction with GPIbα and botrocetin

In order to understand the structural basis of these binding results, we constructed theoretical models for the VWF TASP–GPIbα and VWF TASP–botrocetin bimolecular complexes, as well as for the VWF A1–GPIbα–botrocetin and VWF TASP–GPIbα–botrocetin trimolecular complexes, by using the recently characterized X-ray crystal structures of the GPIbα–VWF A1[15] and VWF A1–botrocetin[16] complexes. Comparison of the binding sites in helices α3 and α4 of the native A1 domain and of helices αII and αI in VWF TASP (Figure 1) shows a good degree of structural similarity of the individual binding sites with a Cα root mean square deviation (RMSD) of 2.8 Å for the grafted residues of helix α3 and 3.4 Å for those of helix α4. Accordingly, the models of the bimolecular GPIbα–VWF TASP and botrocetin–VWF TASP complexes show that VWF TASP reproduces interactions similar to those of the VWF A1 domain (data not shown), although the interaction with the minor binding site of GPIbα (N-terminal part) does not take place as the implicated residues of the VWF A1 domain were not grafted onto VWF TASP.

Analysis of the VWF A1–GPIbα–botrocetin trimolecular complex reveals that the VWF A1 domain binding sites for GPIbα and for botrocetin are ideally oriented relative to each other in the sense that, upon simultaneous binding of GPIbα and botrocetin, a stabilizing interaction surface is created between the C-terminal end of GPIbα and the β subunit of botrocetin (Figure 7A). This interaction will be described in more detail in another paper (Michielin et al., manuscript in preparation). However, an important clash is predicted between GPIbα and botrocetin when both ligands are bound simultaneously to VWF TASP (Figure 7B). This clash results from a difference in the relative orientation of the binding sites for GPIbα and botrocetin: in the VWF A1 domain structure, the α3 and α4 helices form an angle of 31°, whereas this value is only 18° in the VWF TASP model (Figure 1). This 13° change in the relative orientation of the α helices leads to steric hindrance between botrocetin and GPIbα, thereby preventing their simultaneous binding to VWF TASP.

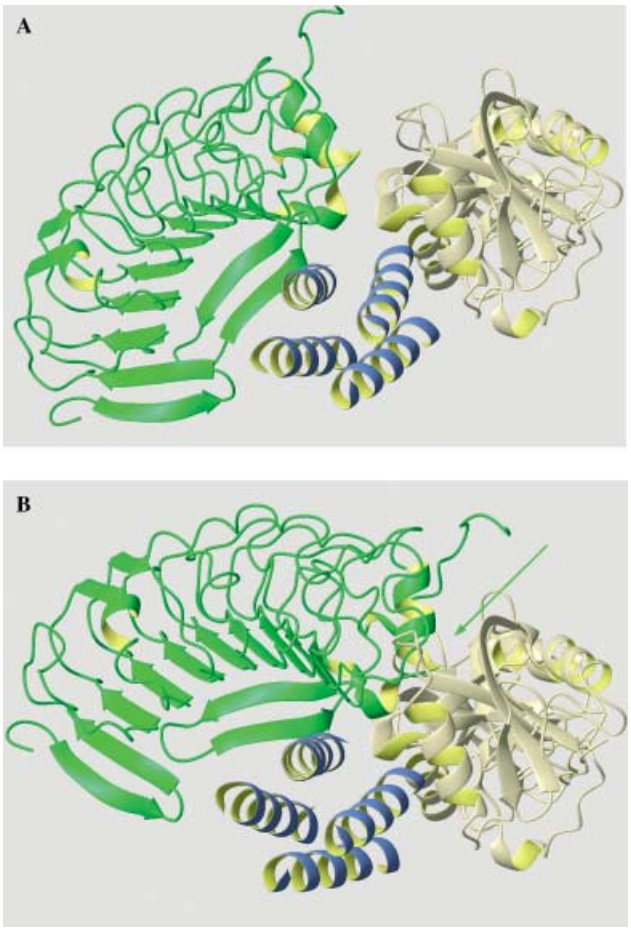

Figure 7. *Docking studies. A) Trimolecular complex of the VWF A1 domain (blue), GPIbα (green), and botrocetin (yellow) shown as ribbons. B) Trimolecular complex between VWF TASP (blue), GPIbα (green), and botrocetin (yellow) shown as ribbons. VWF TASP was superimposed on the A1 domain. The relative orientation of the two VWF TASP binding sites on helices α3 and α4 results in a clash between GPIbα and botrocetin (arrow) that prevents their simultaneous binding to VWF TASP.*

Discussion

The results presented in this manuscript show the functional activity and binding characteristics of VWF TASP, a synthetic four-helix-bundle protein mimicking the surface of the VWF A1 domain. VWF TASP was found to inhibit specifically botrocetin-induced platelet aggregation. Binding studies showed that VWF TASP prevents VWF binding to the GPIb–IX complex by interacting with the VWF binding sites for botrocetin and glycocalicin, the soluble extracellular domain of GPIbα. Docking studies revealed that, although VWF TASP was capable of binding botrocetin or GPIbα separately, it could not bind them simultaneously, because, as a consequence of the relative orientation of the α helices, botrocetin and GPIbα clashed with each other upon binding to VWF TASP.

Biophysical characterization of VWF TASP confirmed its helical structure, which contributed to the stabilization of the individual helices. Several lines of evidence indicate that the effects observed in this study with VWF TASP were specific. First, an unrelated four-helix-bundle TASP, which mimics the surface

area of E-selectin, had no effect in functional or binding tests. This E-selectin TASP was designed according to the same principles as VWF TASP, thereby indicating that the observed effects are not related to the overall helix-bundle conformation of the TASP scaffold, but to grafting of the selected residues in a defined geometry onto the TASP surface. Second, VWF TASP only inhibited platelet responses induced by the interaction of VWF with its ligand, the GPIb–IX complex, since it had no effect on TRAP- or collagen-induced platelet aggregation. Third, a clear dose-response effect was observed with VWF TASP in binding and in functional studies.

The design of VWF TASP, which mimics the three-dimensional structure of helices α3 and α4 of the VWF A1 domain, was carried out on the basis of mutagenesis studies available at the initiation of this project, which hypothesized the presence of a single binding site on the A1 domain.[7,10,12–14] The crystal structures of the GPIbα–VWF A1 complex[15] and the botrocetin–VWF A1 complex[16] confirm that several residues involved in the interactions leading to these complexes have indeed been incorporated into VWF TASP. Most residues described in the major binding site between the A1 domain and the β switch of GPIbα, which are located on helix α3 on top of the A1 domain,[15] have been incorporated into helix αII of VWF TASP. They include Glu596, Lys599, Tyr600, Phe603, Gln604, and Ser 607. Helix αI of VWF TASP contains several residues from helix α4 of the A1 domain that are implicated in the binding of botrocetin to the A1 domain, in particular Arg629, Ser631, and Arg632.[16] Thus, VWF TASP contains several critical residues grafted from helices α3 and α4 of the A1 domain, accounting for the observed interactions of VWF TASP with GPIbα and botrocetin. The interaction between GPIbα and VWF has now been shown to require two binding sites, a large site formed by helix α3, loop α3–β4, and strand β3 and a smaller one formed by loops α1–β3, β3–α2, and α3–β4.[15] The binding tests and the docking studies with VWF TASP indicate that helix α3, located on top of the major binding site, represents a major component of this interaction, since it can, by itself, allow the binding of GPIbα.

Docking studies, based on the X-ray crystal structures of the VWF A1–GPIbα and VWF A1–botrocetin complexes published after the initiation of these studies, allowed us to understand the structural basis of our binding tests, which showed the individual but not simultaneous binding of GPIbα and botrocetin to VWF TASP (Figure 6). These studies confirmed that VWF TASP provided an adequate surface for the individual binding of GPIbα and botrocetin. In contrast to the VWF A1–GPIbα–botrocetin trimolecular complex, VWF TASP could not simultaneously accomodate GPIbα and botrocetin, which were predicted to clash with one another (Figure 7). This clash resulted from a difference in the angle between helices αI and αII of VWF TASP that led to steric hindrance between bound botrocetin and GPIbα. Although this angle difference prevented simultaneous binding of both ligands, VWF TASP exposes at its surface two distinct and functional binding sites, thereby illustrating the potential of the TASP approach for protein design and mimicry.

Although VWF TASP inhibited binding of GPIbα to VWF, we could not determine in this study why VWF TASP prevented only botrocetin-induced activation of platelets and did not affect platelet activation induced by ristocetin and shear stress. Depending on the relative importance of the interaction of VWF with botrocetin or with GPIbα in mediating the observed effect of VWF TASP, two major hypotheses can be put forward to explain these results. First, if the main effect of VWF TASP is to prevent the interaction of the A1 domain with botrocetin, VWF TASP may be unable to prevent platelet activation induced by ristocetin or shear stress because the binding site of botrocetin on VWF is different from that of ristocetin[7] and GPIbα binding sites exposed during shear stress appear to mimic sites exposed upon ristocetin binding.[6,8] Alternatively, VWF TASP may primarily mediate its effect by preventing the interaction of GPIbα with VWF. Although VWF TASP only inhibited botrocetin-mediated platelet activation, it must be kept in mind that VWF TASP mimics only residues of helix α3 exposed on the top of the major binding domain of A1; other residues of the major binding site located in strand β3 and residues of the minor binding site[15] have not been incorporated into VWF TASP. The contribution and the cooperation between these two binding sites in the formation of the VWF–GPIbα complex under physiological and experimental conditions needs further investigation. The results of the binding tests and of the docking studies with VWF TASP provide additional evidence of the central role of helix α3 in the direct interaction between GPIbα and VWF and confirm that helix α3 should be included as a target in the rational design of an inhibitor of the GPIbα–VWF axis.

These results illustrate the potential of the four-helix-bundle TASP approach as method for de novo protein design and rational drug design. A four-helix-bundle architecture, with its simplicity and symmetry, represents a versatile, stable scaffold for the introduction of functional domains. The stability of such constructions relies on the well-packed ROP core. Key characteristics of this method are that it ensures the formation of a bundle structure independently of the surface residues to be transferred and that it offers a suitable area formed by two neighboring helices for proper spatial arrangement of discontinuous recognition sites. Thus, by allowing for systematic studies of structure–function relationships and molecular recognition processes, TASP surface analogues represent a valuable asset to protein design and mimicry. Clearly, the results obtained with VWF TASP illustrate the potential of the TASP approach for designing novel molecules with antiadhesive and antithrombotic activity.

Experimental Section

Reagents: Protected amino acids, coupling reagents, and resins were obtained from Bachem, Novabiochem, and Propeptide. Chemicals for cleavage and scavengers were purchased from Fluka and SepPack C18 cartridges were obtained from Waters. Prostaglandin E_1 (PGE_1), apyrase (grade VII), bovine serum albumin (BSA), *Bothrops Jararaca* venom, streptavidin-bound horse radish peroxidase (HRP), and *o*-phenylenediamine (OPD) were purchased from Sigma. Ristocetin (Helena), *Echis carinatus sochureki* venom (Latoxan), SDS-PAGE and Western blotting reagents (Bio-Rad), [^{125}I] iodine (Amersham), and Iodogen precoated tubes (Pierce) were obtained

from the designated suppliers. Monoclonal antibody (mAb) SZ2 to GPIb was purchased from Immunotech, and mAb 7E3 to GPIIb–IIIa was donated by Lilley, Switzerland.

VWF TASP design, synthesis, and purification: The design of the VWF TASP was based on the SymROP four-helix-bundle structure.[26] The coordinates of the VWF A1 domain (PDB codes: 1OAK and 1AUQ) and ROP (PDB code: 1ROP) are accessible in the Protein Data Bank. The residue numbering of the A1 domain corresponds to the numbers in the mature VWF subunit, where residue 1 is residue 764 of pre-pro-VWF.[9] Six residues of helix α3 of the A1 domain (Glu596, Lys599, Tyr600, Phe603, Gln604, and Ser607) were incorporated into the helix αII sequence of SymROP A_4L_4 and six residues of helix α4 (Arg629, Ser631, Arg632, Lys642, Lys643, and Lys645) were incorporated into helix αI (Figure 1). The resulting structure was first subjected to 500 steps of steepest-descent energy minimization followed by constant-temperature (300 K) molecular dynamics simulation for 500 ps. An average structure was computed for the last 50 ps and this was finally minimized by a further 500 steps of steepest descent energy minimization. All calculations were done with the CHARMM program[28] with an all-atom force field and an *r*-dependent dielectric value of $\varepsilon = 4r$.

Building blocks, helices, and templates were synthesized manually according to standard procedures of solid-phase peptide synthesis by using Rink amide AM or Sasrin (superacid sensitive) resin and applying the 9-fluorenylmethyloxycarbonyl (Fmoc) strategy. Chemoselectively addressable ligation sites were introduced as orthogonally protected Cys residues and bromoacetic acid moieties. After assembly of the linear template sequence Fmoc-Cys(Trt)-D-Pro-Gly-Cys(S*t*Bu)-Glu(O*t*Bu)-Cys(Trt)-D-Pro-Gly-Cys(S*t*Bu) on an Fmoc-Ala-Sasrin resin (substitution: 0.67 mmol g^{-1}) and removal of the N-terminal Fmoc group, the peptide was cleaved with 1% trifluoroacetic acid (TFA) and cyclized with 7-azabenzotriazole-1-yl-oxy-1,1,3,3-tetramethyluronium-hexafluorophosphate (HATU) in *N*,*N*-dimethylformamide. S*t*Bu groups were then selectively removed with DL-dithiothreitol (DTT) and the resulting cyclic template [T_4–(2SH,2Trt)] was purified by reversed-phase HPLC on a Vydac C18 column (250×46 mm). The overall yield was 11%. The template's chemical integrity was confirmed by electrospray ionization (ESI) MS (M_r = 1461.7). The two-helix blocks αI and αII were synthesized on a Rink amide AM resin. The composition of helix αII was Ac-Lys(Dde)-Asp(O*t*Bu)-Ser(*t*Bu)-Ile-Ala-Gln(Trt)-Phe-Leu-Arg(Pmc)-Tyr(*t*Bu)-His(Trt)-Ala-Lys(Boc)-Glu(O*t*Bu)-Leu-Leu-Arg(Pmc)-Ala-NH_2 and the composition of helix αI was (Acm)SCH_2CO-Arg(Pmc)-Asp(O*t*Bu)-Ile-Ala-Ser(*t*Bu)-Arg(Pmc)-Leu-His(Trt)-Ala-His(Trt)-Ala-Lys(Boc)-Lys(Boc)-Leu-Tyr(*t*Bu)-Lys(Boc)-Ala-Lys(Dde)-NH_2 (Dde = 1-(4,4-dimethyl-2,6-dioxocyclohexyldiene)ethyl, Pmc = 2,2,5,7,8-pentamethylchroman-6-sulfonyl, and Boc = *tert*-butoxycarbonyl). The Dde protecting groups were selectively removed with 2% hydrazine (3×10 min) and the newly liberated NH_2 groups were functionalized with Br-CH_2COOSu, (Su = N-succinimidyl). Following peptide cleavage from the resin and simultaneous removal of all acid-labile protecting groups with TFA/triisopropylsilane (TIS)/H_2O (95:2.5:2.5 *v*/*v*) over 1.5 h, the helical blocks were purified by reversed-phase HPLC (30% overall yield) and their chemical integrity was determined by ESI MS (M_W of αI = 2321.5; M_r of αII = 2371.6).

The following method was used for attachment of α helices onto the template. First, αI was dissolved in degassed 0.2 M sodium phosphate buffer (pH 7.4)/acetonitrile (4:1, *v*/*v*), added under argon to a 10 mM solution of the template in acetonitrile, and stirred for 3 h at room temperature. Pure [T_4–(2αI↑,2Trt)] was purified by HPLC. In the next step, the Trt protecting groups were removed by addition of TFA/TIS (80:20, *v*/*v*). After 1 h at room temperature, the peptide was precipitated with diethyl ether. Condensation of αII was performed by using the same conditions employed for αI ligation. After 5 h, [T_4–(2αI↑,2αII↓)] was precipitated with diethyl ether, lyophilized, and isolated from the reaction mixture by SepPack filtration. Subsequently, the Acm protecting group of the N-terminal thioglycolic acid in αII was cleaved with silver triflate in TFA and anisole. After 3 h, the precipitate was dissolved in acetic acid/water/acetonitrile (3:3:2, *v*/*v*), treated with DTT, kept under argon for 3 h, and purified by reversed-phase HPLC. After lyophilization, the TASP was dissolved in 0.1 M $(NH_4)HCO_3$ (pH 8) and the disulfide bridge was formed by air oxidation (M_W = 9838.9).

The CD spectra were recorded on a Jobin Yvon Mark VI circular dichrometer in quartz cells (pathlength = 0.1 cm) with a peptide concentration of 10^{-5} M in phosphate buffer.

Molecular and docking studies:*Model of VWF A1–GPIbα–botrocetin complex*: A model of the VWF A1 domain bound to both 0GPIbα and botrocetin was built by using the VWF A1–GPIbα (PDB code: 1m10) and VWF A1–botrocetin (PDB code: 1ijk) crystal structures.[15,16] The two structures were optimally superimposed by using the corresponding Cα atoms (614–700) of the two VWF A1 domains. The Cα RMSD between the two molecules was low (0.53 Å), which indicates that the conformation of the VWF A1 domain is very similar when complexed with GPIbα or botrocetin. In the resulting VWF A1–GPIbα–botrocetin complex, the C-terminal part of GPIbα has contacts with the β subunit of the botrocetin (Figure 7A). The conformation of the interacting residues was refined by using molecular dynamics simulations with the CHARMM program[28] and $\varepsilon = 4r$.

Model of VWF TASP–GPIbα and VWF TASP–botrocetin complexes: In order to understand how VWF TASP interacts with GPIbα and botrocetin individually, the VWF TASP model was reoriented in the VWF A1–GPIbα X-ray crystal structure (PDB code: 1m10) by optimal superposition of the Cα atoms of the selected residues on helix α3 (Glu596, Lys599, Tyr600, Phe603, Gln604, and Ser607) and in the VWF A1–botrocetin X-ray crystal structure (PDB code: 1ijk) by optimal superposition of the Cα atoms of the selected residues on helix α4 (Arg629, Ser631, Arg632, Lys642, Lys643, and Lys645). The structures for VWF TASP–GPIbα and VWF TASP–botrocetin were minimized and submitted to molecular dynamics simulations of 500 ps each. The average structure for the last 50 ps was again subjected to an energy minimization. An *r*-dependent dielectric constant, $\varepsilon = 4r$, was used for all calculations performed with the CHARMM program.

Model of VWF TASP–GPIbα–botrocetin complex: A model of the VWF TASP–GPIbα–botrocetin complex was obtained in a similar manner to that of the VWF A1–GPIbα–botrocetin complex by using the bimolecular models of the VWF TASP–GPIbα and VWF TASP–botrocetin complexes, that is, the Cα atoms of VWF TASP were used to optimally superimpose the two structures.

Platelet isolation and aggregation: Human blood was obtained from healthy volunteers who had not ingested aspirin for at least ten days. Blood was collected into 0.1 volume of Aster–Jandl anticoagulant. Platelet-rich plasma (PRP) was prepared by centrifugation at 130 *g* for 15 minutes at room temperature. After addition of 1 μM PGE_1, 1 mM aspirin, and 0.15 U mL^{-1} apyrase, PRP was then separated in a centrifuge at 1150 *g* for 15 minutes at room temperature. The platelet pellet was suspended in prewarmed platelet buffer (10 mM 2-[4-2-hydroxyethyl)-1-piperazinyl]ethanesulfonic acid (HEPES), 145 mM NaCl, 5 mM KCl, 2 mM $MgCl_2$, 0.5 mM NaH_2PO_4, 10 mM glucose, 0.3% BSA, pH 7.4) supplemented with 1 μM PGE_1, 1 mM aspirin, and 0.15 U mL^{-1} apyrase and incubated

for 15 minutes at 37 °C. The platelet suspension was centrifuged at 1150 *g* for 10 minutes at room temperature. The pellet was resuspended in platelet buffer at a final concentration of 2×10^8 cells mL^{-1}. This platelet suspension was kept at 37 °C for at least 1 hour before starting activation experiments. Platelet aggregation studies were performed with an APACT 2 aggregometer (LAbor). Washed platelets (2×10^8 mL^{-1}) in platelet buffer supplemented with VWF (10 μg mL^{-1}) and mAb 7E3 (15 μg mL^{-1}) were challenged by the addition of botrocetin (6 μg mL^{-1}) or ristocetin (1.2 mg mL^{-1}).

Proteins: Plasma VWF was purified from the FVIII/VWF concentrate Haemate HS (Centeon) by gel-permeation chromatography with a Sephacryl S1000 column (Pharmacia). The equilibration and elution buffer was 50 mM tris(hydroxymethyl)aminomethane (Tris) with 150 mM NaCl (pH 7.4). Elution fractions containing a single component of >200 kDa were pooled and concentrated by 30% $(NH_4)_2SO_4$ precipitation. Radiolabeled ^{125}I-VWF was prepared by using the Iodogen method (Pierce) according to the recommendations of the manufacturer.

Glycocalicin was isolated from outdated human platelet concentrates (Lausanne Red Cross Transfusion Center) by a procedure derived from Michelson et al. and from Hess et al.[29,30] Briefly, 50 platelet units were sedimented by centrifugation and washed in 10 mM Tris buffer (pH 7.6, washing buffer) containing 150 mM NaCl and 0.6 mM ethylenediaminetetraacetate (EDTA). Platelets were suspended in 3 M KCl and incubated for 30 minutes at 37 °C. The resulting suspension was submitted to high-speed centrifugation (75600 *g*) for 1 hour. The supernatant was extensively dialyzed against washing buffer and applied onto a Wheat Germ Lectin–Sepharose 6B (Pharmacia) column. After washing, the column was eluted with 2.5% *N*-acetyl-D-glucosamine. Elution fractions containing glycocalicin, as assessed by SDS-PAGE/Western blotting (with mAb SZ2) were pooled, dialyzed against Tris buffer (pH 7.6, 20 mM), and applied onto a Q-Sepharose Fast-Flow (Pharmacia) column. After washing, glycocalicin was eluted with a linear NaCl gradient. Elution fractions containing pure glycocalicin were pooled and dialyzed against Tris-buffered saline (TBS). Purified glycocalicin was a single band with an apparent molecular mass of ≈120 kDa by SDS-PAGE and it was recognized on the Western blot by mAb SZ2. Purified glycocalicin inhibited botrocetin-induced platelet aggregation in a dose-dependent manner.

Two-chain botrocetin was purified from crude *Bothrops Jararaca* venom by ion-exchange chromatography on a diethylaminoethyl–Sepharose CL-6B (Pharmacia) column.[31] The presence of botrocetin platelet-aggregating activity was assessed by using a suspension of washed platelets (10^8 mL^{-1}) supplemented with purified VWF (5 μg mL^{-1}). By SDS-PAGE, purified botrocetin was one major band at ≈28 kDa under nonreducing conditions and a doublet near 15 kDa under reducing conditions. Echicetin was purified from crude *Echis carinatus sochureki* venom by affi-gel heparin (Bio-Rad) and hydroxyapatite (Bio-Rad) chromatography as described by Andrews et al.[4]

Protein content was determined by the Micro BCA protein assay (Pierce) with BSA as the standard. Biotinylation of VWF, botrocetin, and glycocalicin was performed with sulfosuccinimidyl-6-(biotinamido) hexanoate (sulfo-NHS-LC-Biotin; Pierce) according to the instructions of the manufacturer. Briefly, proteins (0.3–0.5 mg mL^{-1}) in $NaHCO_3$ (50 mM, pH 8.5) were allowed to react for 2 h at 4 °C with a 20–30 molar excess of biotinylation reagent. The excess reagent was then removed by dialysis against phosphate-buffered saline.

Binding of ^{125}I-VWF to washed platelets: ^{125}I-VWF (6 μg mL^{-1}) was added to a washed platelet suspension (150 μL at 2×10^7 mL^{-1} in platelet buffer) before the addition of botrocetin (2.5 μg mL^{-1}). After incubation for 30 minutes at room temperature, samples were centrifuged at 15600 *g* for 3 minutes and the supernatant was discarded. Radioactivity in the pellets was measured by γ counting. For inhibition studies, inhibitors were added to the samples before the addition of botrocetin. Maximal binding (100%) was defined as binding in the absence of inhibitor. Nonspecific binding (0%) was defined as binding in the absence of botrocetin.

Solid-phase assay: Binding of VWF to immobilized glycocalicin and binding of botrocetin or glycocalicin to immobilized VWF TASP was demonstrated by an ELISA-derived method in 96-well plates. Plates were coated with VWF TASP (40 μg mL^{-1}) or glycocalicin (40 μg mL^{-1}) in 100 mM $NaHCO_3$ overnight at 37 °C in a wet chamber. Wells were then blocked with 2% BSA in TBS with 0.1% Tween 20 (TBS-T) for 1 hour at 37 °C and washed with TBS-T. Biotinylated proteins at various concentrations in TBS-T were added to the coated wells and incubated for 4 hours at room temperature under gentle stirring. After washing, the presence of biotinylated proteins was revealed by the addition of streptavidin-bound HRP followed by OPD development. Coloration intensity was measured at 490 nm in a microplate reader (MR5000, Dynatech). For inhibition experiments, inhibitors were added to the samples before the incubation step.

Acknowledgements

This work was supported by grants 3200-049805 and 328-05632/97 from the Swiss National Science Foundation. The authors thank Sylvain Giraud for helpful discussions and Kimberly Burns for critical reading of the manuscript, the numerous volunteers who donated blood for platelet isolation, and the Centre de Transfusion Sanguine for providing us with outdated platelets. Lilley, Switzerland, is thanked for their kind gift of monoclonal antibodies.

Keywords: botrocetin · molecular modeling · protein design · template synthesis · von Willebrand factor

[1] Z. M. Ruggeri, J. A. Dent, E. Saldivar, *Blood* **1999**, *94*, 172–178.
[2] S. Kulkarni, S. M. Dopheide, C. L. Yap, C. Ravanat, M. Freund, P. Mangin, K. A. Heel, A. Street, I. S. Harper, F. Lanza, S. P. Jackson, *J. Clin. Invest.* **2000**, *105*, 783–791.
[3] S. Miyata, Z. M. Ruggeri, *J. Biol. Chem.* **1999**, *274*, 6586–6593.
[4] R. K. Andrews, W. J. Booth, J. J. Gorman, P. A. Castaldi, M. C. Berndt, *Biochemistry* **1989**, *28*, 8317–8326.
[5] M. C. Berndt, C. M. Ward, W. J. Booth, P. A. Castaldi, A. V. Mazurov, R. K. Andrews, *Biochemistry* **1992**, *31*, 11144–11151.
[6] M. De Luca, D. A. Facey, E. J. Favaloro, M. S. Hertzberg, J. C. Whisstock, T. McNally, R. K. Andrews, M. C. Berndt, *Blood* **2000**, *95*, 164–172.
[7] T. Matsushita, D. Meyer, J. E. Sadler, *J. Biol. Chem.* **2000**, *275*, 11044–11049.
[8] J. F. Dong, M. C. Berndt, A. Schade, L. V. McIntire, R. K. Andrews, J. A. Lopez, *Blood* **2001**, *97*, 162–168.
[9] J. E. Sadler, *Annu. Rev. Biochem.* **1998**, *67*, 395–424.
[10] J. Emsley, M. Cruz, R. Handin, R. Liddington, *J. Biol. Chem.* **1998**, *273*, 10396–10401.
[11] R. Celikel, K. I. Varughese, Madhusudan, A. Yoshioka, J. Ware, Z. M. Ruggeri, *Nat. Struct. Biol.* **1998**, *5*, 189–194.
[12] M. A. Cruz, T. G. Diacovo, J. Emsley, R. Liddington, R. I. Handin, *J. Biol. Chem.* **2000**, *275*, 19098–19105.

[13] S. Vasudevan, J. R. Roberts, R. A. McClintock, J. A. Dent, R. Celikel, J. Ware, K. I. Varughese, Z. M. Ruggeri, *J. Biol. Chem.* **2000**, *275*, 12763 – 12768.
[14] S. Miura, T. G. Diacovo, M. R. Wardell, J. E. Sadler, *Blood* **2000**, *96*, 623a (abstract).
[15] E. G. Huizinga, S. Tsuji, R. A. Romijn, M. E. Schiphorst, P. G. de Groot, J. J. Sixma, P. Gros, *Science* **2002**, *297*, 1176 – 1179.
[16] K. Fukuda, T. A. Doggett, L. A. Bankston, M. A. Cruz, T. G. Diacovo, R. C. Liddington, *Structure (Camb.)* **2002**, *10*, 943 – 950.
[17] E. G. Huizinga, A. Schouten, R. A. P. Romijn, R. K. Andrews, M. C. Berndt, J. Kroon, J. J. Sixma, P. Gros, *Thromb. Haemostasis* **2001**, *85*, OC80 (abstract).
[18] P. A. Nygren, M. Uhlen, *Curr. Opin. Struct. Biol.* **1997**, *7*, 463 – 469.
[19] A. Skerra, *J. Mol. Recognit.* **2000**, *13*, 167 – 187.
[20] M. Mutter, G. Tuchscherer, *Cell. Mol. Life Sci.* **1997**, *53*, 851 – 863.
[21] G. Tuchscherer, L. Scheibler, P. Dumy, M. Mutter, *Biopolymers* **1998**, *47*, 63 – 73.
[22] G. Tuchscherer, D. Grell, M. Mathieu, M. Mutter, *J. Pept. Res.* **1999**, *54*, 185 – 194.
[23] D. W. Banner, M. Kokkinidis, D. Tsernoglou, *J. Mol. Biol.* **1987**, *196*, 657 – 675.
[24] T. Matsushita, J. E. Sadler, *J. Biol. Chem.* **1995**, *270*, 13406 – 13414.
[25] P. A. Kroner, A. B. Frey, *Biochemistry* **1996**, *35*, 13460 – 13468.
[26] D. Grell, J. S. Richardson, D. C. Richardson, M. Mutter, *J. Mol. Graph. Model.* **2000**, *18*, 290 – 298; D. Grell, J. S. Richardson, D. C. Richardson, M. Mutter, *J. Mol. Graph. Model.* **2000**, *18*, 309 – 310.
[27] G. Tuchscherer, C. Lehmann, M. Mathieu, *Angew. Chem.* **1998**, *110*, 3160 – 3164; *Angew Chem. Int. Ed.* **1998**, *37*, 2990 – 2993.
[28] B. R. Brooks, R. E. Bruccoleri, B. D. Olafson, J. D. States, S. Swaminathan, M. Karplus, *J. Comput. Chem.* **1983**, *4*, 187 – 217.
[29] A. D. Michelson, J. Loscalzo, B. Melnick, B. S. Coller, R. I. Handin, *Blood* **1986**, *67*, 19 – 26.
[30] D. Hess, J. Schaller, E. E. Rickli, K. J. Clemetson, *Eur. J. Biochem.* **1991**, *199*, 389 – 393.
[31] Y. Fujimura, K. Titani, Y. Usami, M. Suzuki, R. Oyama, T. Matsui, H. Fukui, M. Sugimoto, Z. M. Ruggeri, *Biochemistry* **1991**, *30*, 1957 – 1964.

Received: November 20, 2003

